Calculation of Transonic Flows Over Bodies of Varying Complexity Using Slender Body Theory

Karunamurthy Rajagopal*
University of California, Santa Barbara, California
Norman D. Malmuth†
Rockwell International Science Center, Thousand Oaks, California
and
Wilbert J. Lick‡
University of California, Santa Barbara, California

Transonic flows over several bodies of varying complexity, including a simple wing-body combination and the Shuttle Orbiter, have been modeled with the use of slender body theory. In the theory, the original three-dimensional problem is divided into two simpler component problems, the near field and the far field. The near field problem represents a crossflow that is almost incompressible and is defined by Laplace's equation with a flow tangency boundary condition on the body. A nonlinear transonic small disturbance approximation is the basis for the far-field problem and describes the flow over a body of revolution having the same longitudinal area distribution as the asymmetric body. Both the near- and far-field problems are two-dimensional boundary value problems. A boundary-element method is used to solve the near-field problem. The solution for the axisymmetric far-field problem is obtained by a successive line overrelaxation method. The two component solutions are combined to obtain the complete solution. Flows with various angles of attack and zero sideslip have been considered. Also, some off-body flow calculations were conducted. For attached flows, the calculations predicted the pressure results with good accuracy.

Nomenclature

A = reduced normalized body cross-sectional area
a = local speed of sound
B_w = wing span
b = characteristic lateral dimension
C_P = pressure coefficient
c = reference length
d_j = length of boundary element j
F = dimensionless radius defined in Eq. (5)
g^* = Mach number-dependent part of inner peturbation potential
K = transonic similarity parameter
L = effective Orbiter length
M_∞ = freestream Mach number
N = number of boundary elements
n = outward normal to body contour in crossflow plane
P_{ij}, Q_{ij} = matrix elements in Green's formula method
R_i = column matrix element in Green's formula method
r = R/c
$\bar{r}$ = $\delta R/c$
r^* = $R/\delta c$
r_{PQ} = vector connecting point P to point Q
S^*, S = source strengths in Eqs. (4) and (19), respectively
U_∞ = freestream velocity
x = X/L
X, R, Θ = dimensional cylindrical coordinates, shown in Fig. 1
X, Y, Z = dimensional Cartesian coordinates, shown in Fig. 1
y^* = $Y/\delta c$
y', z' = local crossflow coordinates, shown in Fig. 2
z^* = $Z/\delta c$
α = angle of attack
γ = ratio of specific heats
δ = characteristic thickness ratio of body
η = dimensionless span location, $2Z/B_W$
ξ = dummy variable for x in Eq. (29)
Φ = velocity potential
ϕ, ϕ^* = outer and inner representation of perturbation potential, respectively
ϕ_2^* = Mach number-independent part of inner perturbation potential

Subscripts

B = body
inner = near field
outer = far field

Special Symbols

log = logarithm
$d\Gamma$ = boundary of region Γ

Introduction

TRANSONIC slender body theory[1-4] has been used by many researchers for simple cases of the flow around elliptic cone cylinders, thin triangular wings, and projectiles. Malmuth et al.[5] treated the Shuttle aerodynamics for zero angle of attack using this theory and reported some preliminary pressure results for near-sonic supersonic Mach numbers. The present work treats many geometries, including the Orbiter, and incorporates efficient computational methods. The intent is to provide a design-oriented, rapid, and computationally efficient procedure with the capability of predicting transonic flows.

Essentially, the theory reduces the original three-dimensional problem of the flow over a body to the solution of two

Received July 27, 1987; presented as Paper 88-0005 at the AIAA 26th Aerospace Sciences Meeting, Reno, NV, Jan. 11-14, 1988; revision received April 4, 1988.

*Post-Doctoral Researcher, Department of Mechanical Engineering. Member AIAA.
†Member of Technical Staff. Associate Fellow AIAA.
‡Professor, Department of Mechanical Engineering.

component problems, each of which is two-dimensional and, hence, simpler. As a first step to achieve the simplification, the velocity potential is expanded asymptotically in both the near and far field from the body. Substituting these expansions (which are obtained from transonic slender body theory) into the full potential equation gives two boundary value problems for both regions. The differential equation for the near-field flow, with is an incompressible crossflow, is Laplace's equation and is subject to a flow tangency boundary condition on the body. On the other hand, a nonlinear transonic small disturbance equation is obtained as an approximation for the far field. This outer flow is the flow over a body of revolution with the same axial area distribution as the original body.

Both of these boundary value problems are two-dimensional. To solve the near-field Laplace's equation, it was decided to use a boundary-element technique. The far-field nonlinear transonic small disturbance equation was solved by a successive line overrelaxation procedure. Different elements of the complete pressure solution were obtained from the near- and far-field solutions and combined to provide the total loading. This procedure can predict results for flows with zero sideslip and nonzero angles of attack and is also capable of off-body pressure and velocity computations.

Mathematical Formulation

Consider the cylindrical coordinate system (X,R,Θ) fixed in the body, as illustrated in Fig. 1. In this coordinate system, the velocity potential equation, valid for a compressible, steady, irrotational, isentropic flow, is

$$(a^2-\Phi_X^2)\Phi_{XX}+(a^2-\Phi_R^2)\Phi_{RR}+a^2\Phi_R/R + (a^2-\Phi_\Theta^2/R^2)\Phi_{\Theta\Theta}/R^2-2\Phi_X\Phi_R\Phi_{XR} - 2\Phi_X\Phi_\Theta\Phi_{X\Theta}/R^2-2\Phi_R\Phi_\Theta\Phi_{R\Theta}/R^2=0 \quad (1)$$

where the velocity potential Φ is defined such that its derivative in a given direction yields the velocity in that direction, and the subscripts denote partial differentiation. The expression for the pressure coefficient C_P is given by

$$C_P=\frac{2}{\gamma M_\infty^2}\left\{\left[1+\frac{\gamma-1}{2}M_\infty^2\frac{U_\infty^2(1+\alpha^2)-Q^2}{U_\infty^2}\right]^{\gamma/(\gamma-1)}-1\right\} \quad (2)$$

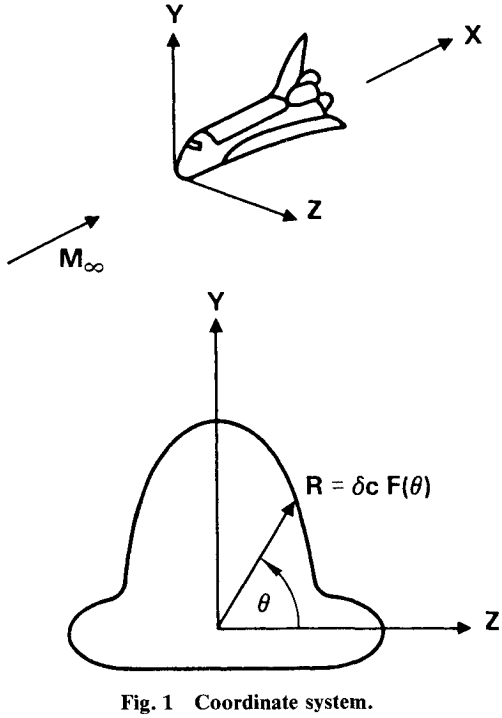

Fig. 1 Coordinate system.

where

$$Q^2=\Phi_X^2+\Phi_R^2+(\Phi_\Theta/R)^2 \quad (3)$$

Instead of solving the three-dimensional full potential equation [Eq. (1)], a simpler set of two equations will be solved. These simpler equations are obtained from transonic slender body theory. In the theory, the velocity potential representing the flow is expanded asymptotically[6,7] in terms of the thickness ratio in the regions close to the body (near field) and far away from the body (far field). The validity of the expansions improves for Mach number close to unity, i.e., for transonic Mach numbers. The theory is also applicable in the transonic range to configurations that are not necessarily slender. This is because the crossflow in planes normal to the freestream direction always tends to be incompressible when $M_\infty \to 1$. With the substitution of the expansions in the full potential equation, the near- and far-field problems are defined in terms of simpler differential equations. By examining the nature of the solutions for these equations and by matching the near- and far-field expansions in the overlap zone of validity, the unknown elements in the expansions are determined. Finally, the surface pressure distribution is obtained from the perturbation potential.

Inner Expansion

The appropriate asymptotic expansion for the velocity potential in the inner (near-field) region for the case of zero sideslip is [1,3]

$$\Phi_{\text{inner}}=U_\infty[x+\alpha r\sin\theta+(\delta^2\log\delta)2\,S^*(x)+\delta^2\phi^*(x,r^*,\theta) + O(\delta^4)] \quad (4)$$

which holds in an inner limit,

$$\left.\begin{aligned} x &= X/c \\ r^* &= R/\delta c \\ K &= (1-M_\infty^2)/\delta^2 \\ A &= \alpha/\delta \\ B &= b/\delta \end{aligned}\right\} \text{fixed as } \delta\to 0$$

where b is a nondimensional span or aspect ratio parameter, δ a maximum thickness ratio (i.e., the ratio of the maximum diameter of the axisymmetric equivalent body with the same axial area distribution as the original body to the length of the body), and S^* a source strength to be determined later. In this inner limit, r^* is fixed as $\delta\to 0$. According to this limit, if δ becomes small, R should also become small. Thus, the body geometry will be preserved in this limit. The term containing $\delta^2\log\delta$ is inserted for purposes of matching and arises because of the logarithmic behavior of the solution.

If the equation of the cross-sectional shape of the body in an x-const plane is given by (refer to Fig. 1)

$$R=\delta c F(x,\theta) \quad (5)$$

the cross-sectional area $A(x)$ is then

$$A=\int F^2\,d\theta \quad (6)$$

where the integral is around the cross-sectional contour.

On substituting Eq. (4) into the full potential equation [Eq. (1)] and retaining only terms of order 1, a boundary-value problem for the Mach number-independent part of the inner perturbation potential ϕ^*, denoted as ϕ_2^*, is obtained. The theory shows that near the body, the crossflow described by the Mach number-independent perturbation potential ϕ_2^* is

incompressible in the sense that it satisfies Laplace's equation

$$\nabla^2\phi_2^* = r^*\frac{\partial}{\partial r^*}\left(r^*\frac{\partial\phi_2^*}{\partial r^*}\right) + \frac{\partial^2\phi_2^*}{\partial\theta^2} = 0 \tag{7}$$

The condition of tangency of the flow to the body surface gives the Neumann boundary condition as

$$\frac{\partial\phi_2^*}{\partial n} = \frac{FF_x - (\alpha/\delta)F\sin\theta + (\alpha/\delta)F_\theta\cos\theta}{\sqrt{F^2+F_\theta^2}} \tag{8}$$

where F is as defined in Eq. (5) The boundary condition in Cartesian coordinates is

$$\frac{\partial\phi_2^*}{\partial n} = \frac{y_x^* - \alpha/\delta}{\sqrt{1+(y_z^*)^2}} = \frac{z_x^* + (\alpha/\delta)z_y^*}{\sqrt{1+(z_y^*)^2}} \tag{9}$$

where

$$y^* = Y/\delta c \text{ and } z^* = Z/\delta c \tag{10}$$

The far field of ϕ_2^* is asymptotically a source flow in the sense that

$$\phi_2^* = S^*(x)\log r^* \quad \text{as } r^*\to\infty \tag{11}$$

Alternatively, by representing ϕ_2^* in terms of simple and double sources on the boundary using Green's theorem, it becomes

$$\phi_2^* = \frac{1}{2\pi}\log r^*\int\frac{\partial\phi_2^*}{\partial n}\,d\Gamma \quad \text{for } r^*\to\infty \tag{12}$$

From Eq. (8),

$$\int\frac{\partial\phi_2^*}{\partial n}\,d\Gamma = A'(x) \tag{13}$$

where the prime denotes differentiation with respect to x. Hence,

$$\phi_2^* = \frac{A'(x)}{2\pi}\log r^* \quad \text{for } r^*\to\infty \tag{14}$$

Now, comparing Eq. (14) with Eq. (11), one obtains

$$S^*(x) = A'(x)/2\pi \tag{15}$$

As previously mentioned, ϕ_2^* is the Mach number-independent part of the inner perturbation potential ϕ^*. Therefore, ϕ^* can be considered to consist of two parts, i.e.,

$$\phi^* = \phi_2^* + g^*(x;K) \tag{16}$$

where the Mach number-dependent function g^* is to be determined by matching with the outer expansion.

Outer Expansion

The appropriate expansion for the velocity potential in the outer (far field) region is [1,3]

$$\Phi_{\text{outer}} = U_\infty[x + \alpha r\sin\theta + \delta^2\phi(x,\bar r;K) + O(\delta^4)] \tag{17}$$

which holds in an outer limit,

$$\left.\begin{matrix}K\\ \bar r = \delta R/c\end{matrix}\right\} \text{fixed as } \delta\to 0.$$

The Mach wave structure of a near-sonic supersonic flow is preserved in this limit. Also, the body shrinks to the axis $\bar r = 0$.

Substitution of Eq. (17) into Eq. (1) and retention of the dominant terms gives

$$[K - (\gamma+1)\phi_x]\phi_{xx} + \frac{1}{\bar r}(\bar r\phi_{\bar r})_{\bar r} = 0 \tag{18}$$

which is the nonlinear transonic small disturbance equation. No attempt has been made in this treatment to employ traditional empirical corrections incorporating powers of the freestream Mach number in the definitions of the transonic small disturbance parameter K, the pressure coefficient, and $\bar r$ in order to improve the agreement with experiment.

For purposes of matching with the inner solution, the behavior of the solution to Eq. (18) as $\bar r\to 0$ is needed. The appropriate solution corresponds to a distribution of singularities on the axis $\bar r = 0$, where the basic distribution is source-like. The disturbance potential ϕ near the body can be written as

$$\phi(X,\bar r;K) = S(x)\log\bar r + g(x;K) \quad \text{for } \bar r\to 0 \tag{19}$$

where S is a source distribution on the line $\bar r = 0$. The function g will be shown later to be the same as g^*. Now, it follows from Eq. (19) that

$$\lim_{\bar r\to 0}(\bar r\phi_{\bar r}) = S(x) \tag{20a}$$

$$g(x;K) = \lim_{\bar r\to 0}[\phi - S(x)\log\bar r] \tag{20b}$$

Matching

In order to match the inner expansion [Eq. (4)] and the outer expansion [Eq. (17)], it is assumed that they are both valid in an overlap region defined by an intermediate class of limits, given as

$$\left.\begin{matrix}K\\ x\\ r_\eta = R/c\eta\end{matrix}\right\} \text{fixed as } \delta\to 0$$

Here the parameter η is such that

$$\delta \ll \eta \ll 1/\delta \tag{21}$$

Thus, the matching takes place as

$$r^* = \frac{\eta r_\eta}{\delta}\to\infty \tag{22a}$$

$$\bar r = \delta\eta r_\eta\to 0 \tag{22b}$$

The behavior of the inner solution as $r^*\to\infty$ must agree with the behavior of the outer solution as $\bar r\to 0$. From matching, the unknown terms are determined to be

$$S(x) = S^*(x) = A'(x)/2\pi \tag{23a}$$

$$g(x;K) = g^*(x;K) \tag{23b}$$

Thus, Eqs. (20a) and (20b) become

$$\lim_{\bar r\to 0}(\bar r\phi_{\bar r}) = A'(x)/2\pi \tag{24a}$$

$$g(x;K) = \lim_{\bar r\to 0}\left[\phi - \frac{A'(x)}{2\pi}\log\bar r\right] \tag{24b}$$

and the inner potential beomes

$$\Phi_{\text{inner}} = U_\infty\{x + \alpha r\sin\theta + (\delta^2\log\delta)A'(x)/\pi + \delta^2[\phi_2^* + g(x;K)]\} \tag{25}$$

Finally, with the substitution of this inner expansion, Eq. (2)

becomes

$$C_P = -\delta^2\left[2\frac{\partial\phi_2^*}{\partial x} + \left(\frac{\partial\phi_2^*}{\partial y^*}\right)^2 + \left(\frac{\partial\phi_2^*}{\partial z^*}\right)^2 + 2\frac{\alpha}{\delta}\frac{\partial\phi_2^*}{\partial y^*} + \frac{2}{\pi}(\log\delta)\,A''(x) + 2g'(x;K)\right] \tag{26}$$

The original three-dimensional problem defined by Eq. (1) has been decomposed into two two-dimensional problems. They are 1) the inner problem, i.e., Eqs. (7) and (8) for the inner perturbation potential ϕ_2^*, and 2) the outer problem, i.e., Eqs. (18) and (24a) for the outer perturbation potential ϕ. Equation (24b) defines the function g, and the pressure is given by Eq. (26). Henceforth, the first four terms in Eq. (26) will be called the "inner solution" and other two terms the "outer solution."

To predict off-body pressure at a point off the body surface, the derivatives of ϕ_2^* in Eq. (26) need to be computed at that point. Also, the off-body velocities nondimensionalized with respect to the freestream velocity are given by

$$\frac{\partial\Phi}{\partial x} = 1 + \delta^2\left[\frac{\partial\phi_2^*}{\partial x} + \frac{1}{\pi}(\log\delta)\,A''(x) + g'(x;K)\right] \tag{27a}$$

$$\frac{\partial\Phi}{\partial y} = \alpha + \delta\frac{\partial\phi_2^*}{\partial y^*} \tag{27b}$$

$$\frac{\partial\Phi}{\partial z} = \delta\frac{\partial\phi_2^*}{\partial z^*} \tag{27c}$$

Numerical Methods

Far-Field Problem

The nonlinear transonic small disturbance equation [Eq. (18)] was solved using successive line overrelaxation (SLOR).[8,9] In addition to Eq. (24a), far-field boundary conditions assumed are

$$\phi = 0,\ r \to \infty \tag{28a}$$

$$\phi_x = 0,\ x \to \pm\infty \tag{28b}$$

Proper smoothing is required for the streamwise cross-sectional area distribution $A(x)$ of the Orbiter. If the noise present in the area input data is not smoothed, large oscillation are present in the first and second derivatives of $A(x)$. The behavior of these derivatives has a large influence on the pressure, as shown in Eqs. (26) and (24b). The IMSL subroutine ICSSCU was used for the smoothing.

In addition to the SLOR approach to the nonlinear problem, the linear analytic solution of the Prandtl-Glauert equation was also obtained (linearized slender body theory). The linear equation is obtained when $(\gamma+1)\phi_x$ is negligible compared to K in Eq. (18) and is valid for subsonic and supersonic flows leaving out the transonic range. For supersonic flows, the expression for g is given by the von Kármán line source formula as[10]

$$g(x;K) = \frac{A'(x)}{2\pi}\log\frac{\sqrt{-K}}{2} - \frac{1}{2\pi}\int_0^x A''(\xi)\log(x-\xi)\,d\xi - \frac{1}{2\pi}A'(0)\log(x) \tag{29}$$

Equation (29), although valid only for supersonic flows, is useful to check the accuracy of the nonlinear theory algorithm at moderate supersonic Mach numbers.

Near-Field Problem

The near-field Neumann boundary value problem [Eqs. (7-9)] was solved by a boundary-element technique. Comprehensive descriptions of this method can be found in Jaswon and Symm,[11] Brebbia,[12] and Brebbia et al.[13] It has the advantage of reducing the dimensionality of the problem by one and is especially suited for cases where the solution is mainly desired on the boundaries. Two different versions of the technique were studied in an earlier work by the authors[14]: 1) the indirect approach using hypothetical source panels on the boundary, and 2) the direct method employing Green's formula. This study concluded that the Green's formula method was robust and more accurate than the source panel method. Hence the present work employs the former, whereas the source panel method was used in Ref. 5. In this section, the superscript * on y and z is dropped for convenience. Also, for the same reason, ϕ_2^* is written simply as ϕ.

With reference to Fig. 2, the boundary can be considered to consist of N straight-lined elements with piecewise constant properties (with the jth element being the one connecting the nodes j and $j+1$ and with the potential ϕ_j and the flux ϕ_{n_j}). Here, a form of Green's formula[15] can be used to express the potential ϕ_i at the point P in terms of the potentials ϕ_j and the fluxes ϕ_{n_j} on the boundary elements as

$$\phi_i + \sum_{j=1}^{N}\phi_j\int\frac{1}{2\pi}\frac{\partial\log r_{PQ}}{\partial n_j}\,d\Gamma_j = \sum_{j=1}^{N}\phi_{n_j}\int\frac{1}{2\pi}\log r_{PQ}\,d\Gamma_j \tag{30}$$

This equation can be written as

$$\phi_i + \sum_{j=1}^{N}P_{ij}\phi_j = \sum_{j=1}^{N}Q_{ij}\phi_{n_j} \tag{31}$$

where

$$P_{ij} = -\frac{1}{2\pi}\left(\tan^{-1}\frac{z'+d_j/2}{y'} - \tan^{-1}\frac{z'-d_j/2}{y'}\right) \tag{32}$$

$$Q_{ij} = \frac{1}{4\pi}\Big\{(z'+d_j/2)\log[(z'+d_j/2)^2+y'^2] - (z'-d_j/2)\log[(z'-d_j/2)^2+y'^2] - 2d_j + 2y'\left(\tan^{-1}\frac{z'+d_j/2}{y'} - \tan^{-1}\frac{z'-d_j/2}{y'}\right)\Big\} \tag{33}$$

Equation (31) for $i = 1,2,\ldots N$ can be put in matrix form as

$$\boldsymbol{P}\phi = \boldsymbol{Q}\phi_n = \boldsymbol{R} \tag{34}$$

The diagonal element in the matrix $\boldsymbol{P}$ is equal to 0.5. Moreover, this term can be checked for accuracy using the following condition[13]:

$$P_{ii} = 1.0 - \sum_{\substack{j=1\\ j\neq i}}^{n}P_{ij} \quad i = 1,2,\ldots,N \tag{35}$$

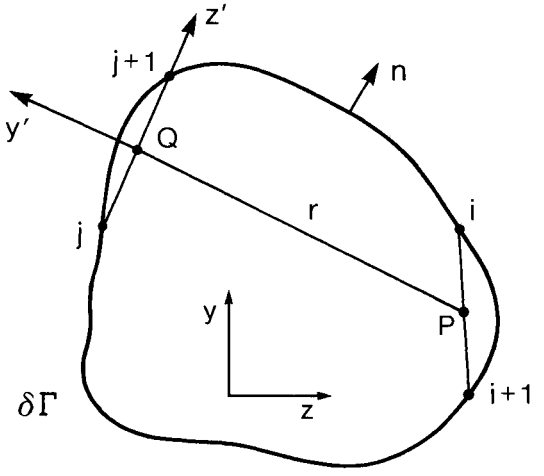

Fig. 2 Schematic of a boundary.

Now, knowing the vector ϕ_n in Eq. (34), the vector R is calculated by matrix mutliplication. Then, the vector ϕ is obtained by solving the linear system of equations $P\phi = R$ using the IMSL subroutine LEQT1F.

Most of the preceding equations are in terms of z' and y', the coordinates of the point P with respect to the local coordinate system on the boundary element. These coordinates are obtained from the global coordinates z and y by the following relations:

$$z'_P = [(z_P - z_Q)(z_{j+1} - z_j) + (y_P - y_Q)(y_{j+1} - y_j)]/d_j \quad (36)$$

$$y'_P = [(y_P - y_Q)(z_{j+1} - z_j) - (z_P - z_Q)(y_{j+1} - y_j)]/d_j \quad (37)$$

where the subscripts P and Q refer to points P and Q in Fig. 2.

To enable the calculation of the gradients ϕ_y and ϕ_z, Eq. (30) can be differentiated and the following expressions can be obtained:

$$\frac{\partial \phi_i}{\partial y} = -\sum_{j=1}^{N} \phi_j \left[\frac{\partial P_{ij}}{\partial y'} \left(\frac{z_{j+1} - z_j}{d_j} \right) + \frac{\partial P_{ij}}{\partial z'} \left(\frac{y_{j+1} - y_j}{d_j} \right) \right] + \sum_{j=1}^{N} \phi_{n_j} \left[\frac{\partial Q_{ij}}{\partial y'} \left(\frac{z_{j+1} - z_j}{d_j} \right) + \frac{\partial Q_{ij}}{\partial z'} \left(\frac{y_{j+1} - y_j}{d_j} \right) \right] \quad (38)$$

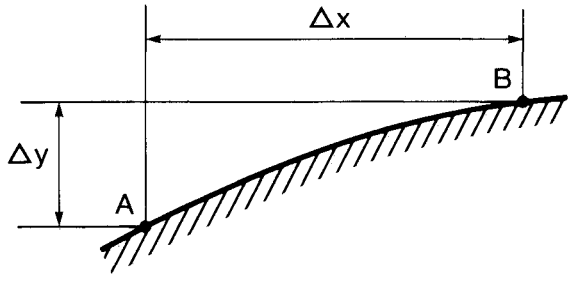

Fig. 3 Body surface in a z = const plane.

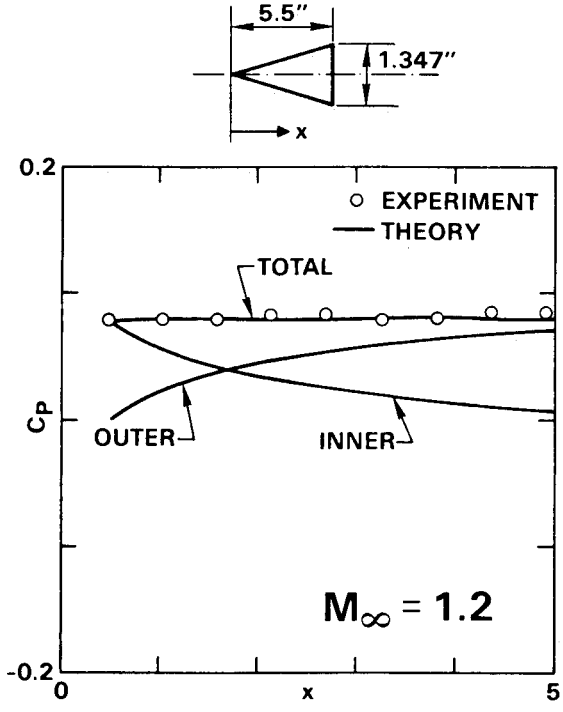

Fig. 4 Flow over a circular cone; $M_\infty = 1.2$.

$$\frac{\partial \phi_i}{\partial z} = -\sum_{j=1}^{N} \phi_j \left[\frac{\partial P_{ij}}{\partial y'} \left(\frac{y_j - y_{j+1}}{d_j} \right) + \frac{\partial P_{ij}}{\partial z'} \left(\frac{z_{j+1} - z_j}{d_j} \right) \right] + \sum_{j=1}^{N} \phi_{n_j} \left[\frac{\partial Q_{ij}}{\partial y'} \left(\frac{y_j - y_{j+1}}{d_j} \right) + \frac{\partial Q_{ij}}{\partial z'} \left(\frac{z_{j+1} - z_j}{d_j} \right) \right] \quad (39)$$

where

$$\frac{\partial P_{ij}}{\partial y'} = \frac{1}{2\pi} \left[\frac{z' + d_j/2}{(z' + d_j/2)^2 + y'^2} - \frac{z' d_j/2}{(z' - d_j/2)^2 + y'^2} \right] \quad (40a)$$

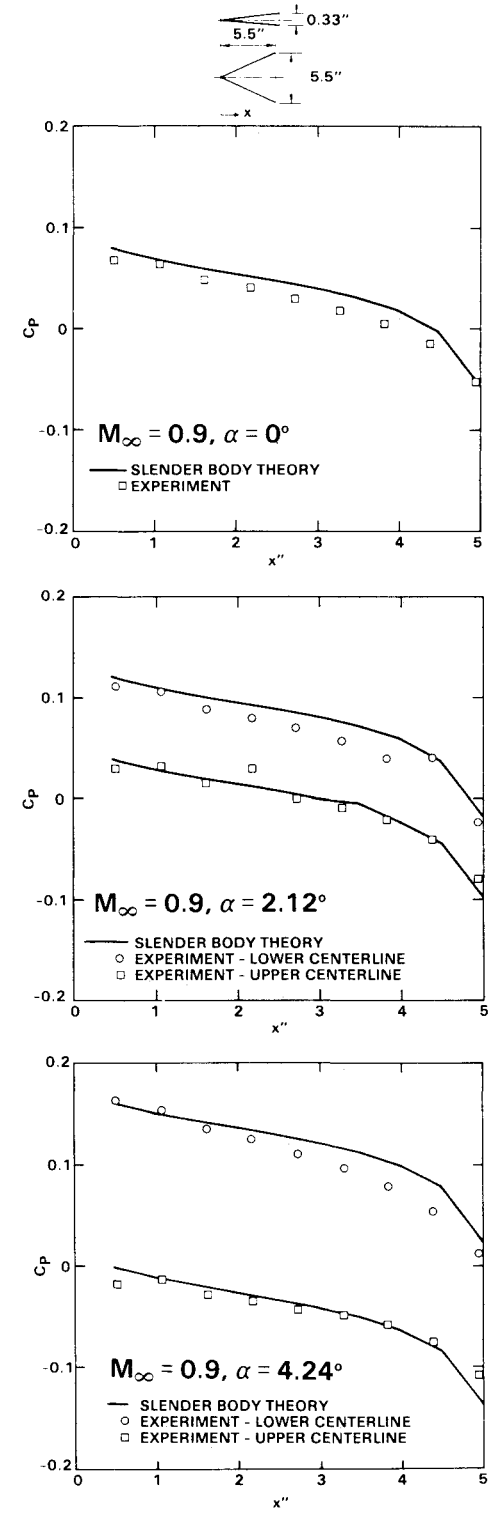

Fig. 5 Flow over an elliptic cone for various angles of attack; $M_\infty = 0.9$.

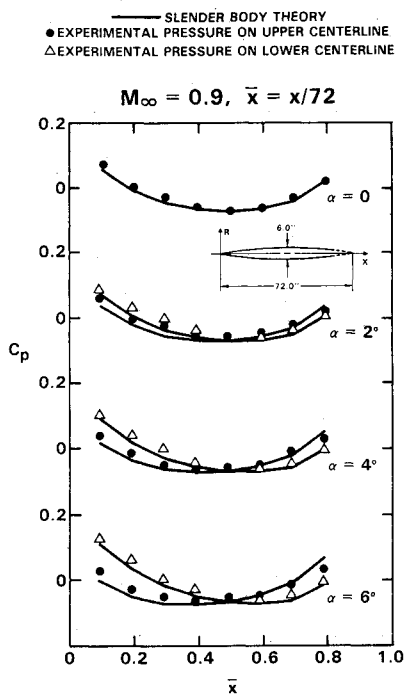

Fig. 6 Flow over an parabolic arc of revolution body for various angles of attack; $M_\infty = 0.9$.

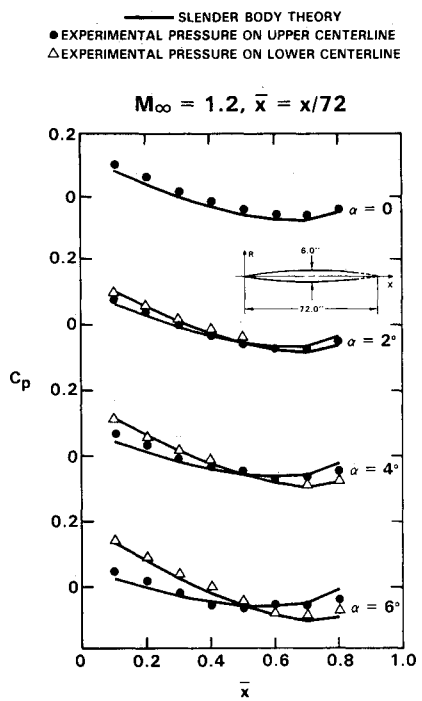

Fig. 7 Flow over a parabolic arc of revolution body for various angles of attack; $M_\infty = 1.2$.

$$\frac{\partial P_{ij}}{\partial z'} = -\frac{y'}{2\pi}\left[\frac{1}{(z'+d_j/2)^2+y'^2} - \frac{1}{(z'-d_j/2)^2+y'^2}\right] \quad (40b)$$

$$\frac{\partial Q_{ij}}{\partial y'} = \frac{1}{2\pi}\left[\tan^{-1}\frac{z'+d_j/2}{y'} - \tan^{-1}\frac{z'-d_j/2}{y'}\right] \quad (40c)$$

$$\frac{\partial Q_{ij}}{\partial z'} = \frac{1}{4\pi}\log\left[\frac{(z'+d_j/2)^2+y'^2}{(z'-d_j/2)^2+y'^2}\right] \quad (40d)$$

To complete the calculation of the inner solution, the partial derivative ϕ_x is yet to be determined. In Fig. 3, the difference

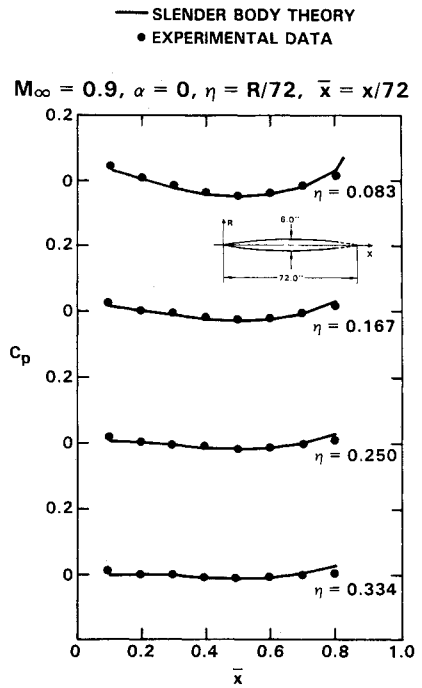

Fig. 8 Off-body results for parabolic arc of revolution body; $M_\infty = 0.9$.

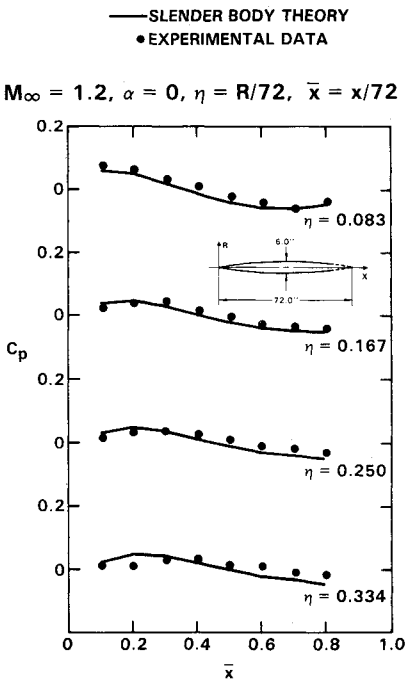

Fig. 9 Off-body results for parabolic arc of revolution body; $M_\infty = 1.2$.

between ϕ values at B and A in a plane z = const is given by

$$\phi_B - \phi_A = (\phi_x)_A \cdot \Delta x + (\phi_y)_A \cdot \Delta y \quad (41)$$

Knowing ϕ and ϕ_y obtained from the Laplace equation solver, ϕ_x can be computed. In certain sections of the boundary, such as the vertical fuselage surface and the wing tip, this calculation is implemented in a plane y = const for accuracy.

Results

The slender body code was used to predict the flow over a circular cone, an elliptic cone, a parabolic arc of revolution

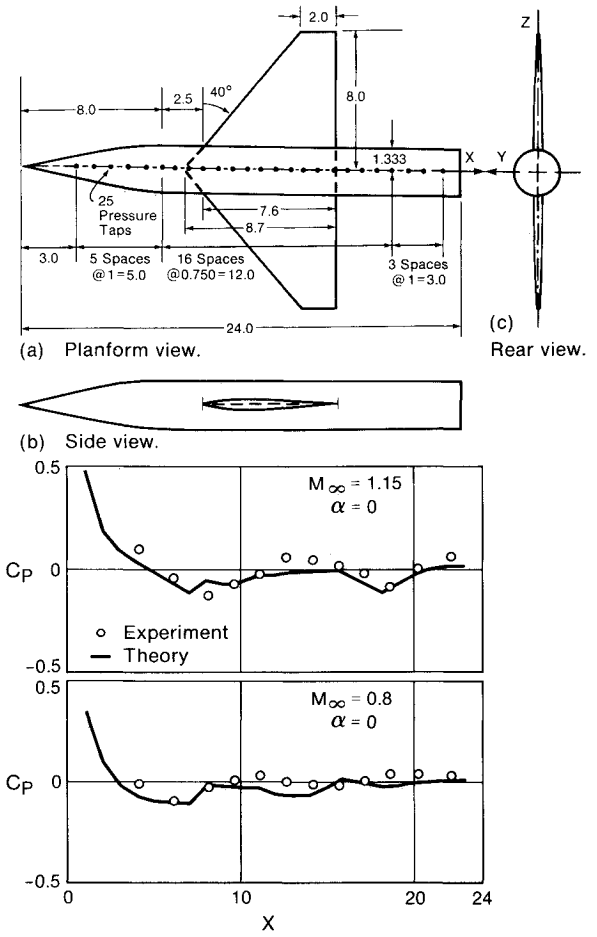

Fig. 10 Flow over a simple wing-body combination; $M_\infty = 1.15$ and $M_\infty = 0.8$.

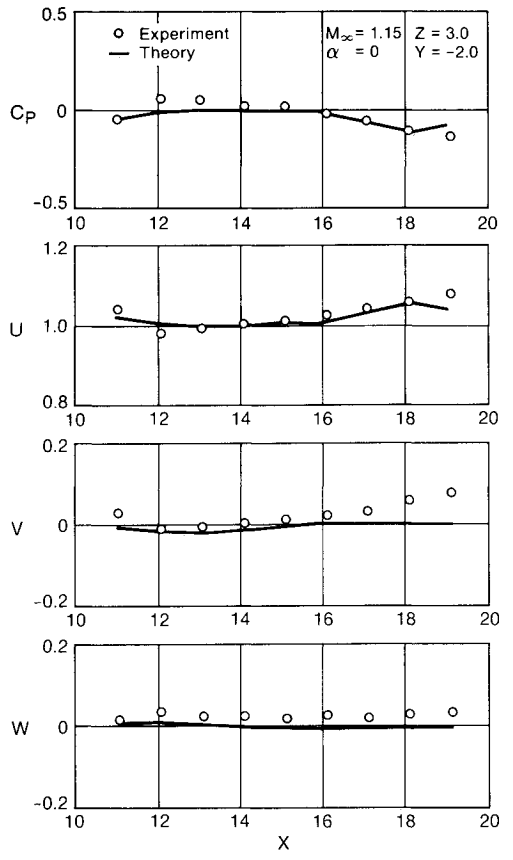

Fig. 11 Off-body results for wing-body combination; $M_\infty = 1.15$.

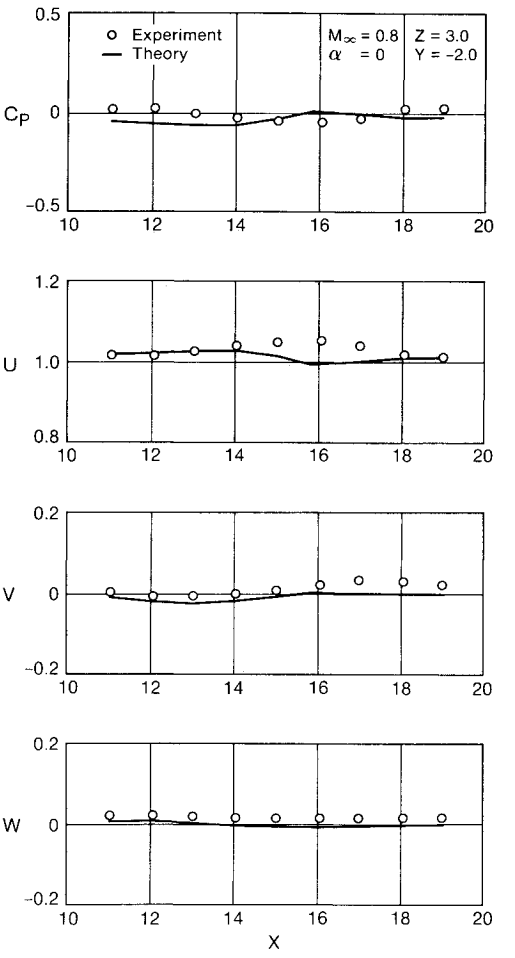

Fig. 12 Off-body results for wing-body combination; $M_\infty = 0.8$.

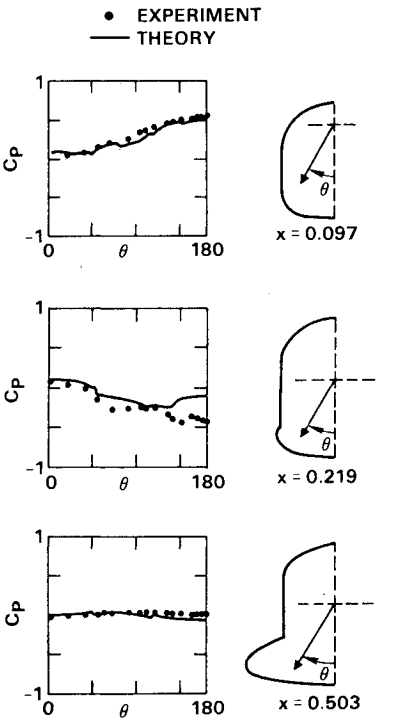

Fig. 13 Circumferential pressure distribution on Shuttle fuselage; $M_\infty = 1.25$.

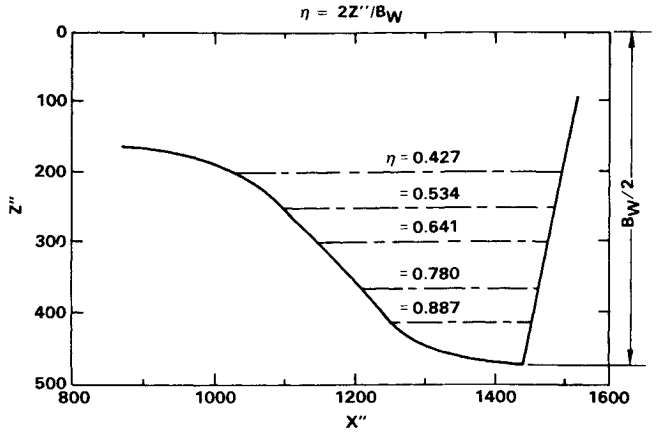

Fig. 14 Schematic of Orbiter wing with various chordwise span stations.

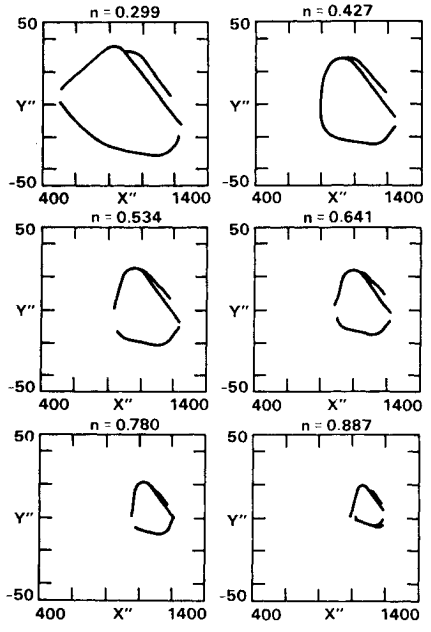

Fig. 15 Modification in wing surface at various span stations; $M_\infty = 1.25$.

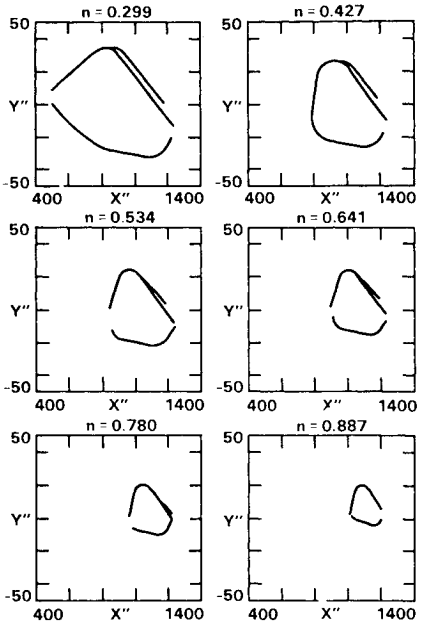

Fig. 16 Modification in wing surface at various span stations; $M_\infty = 0.9$.

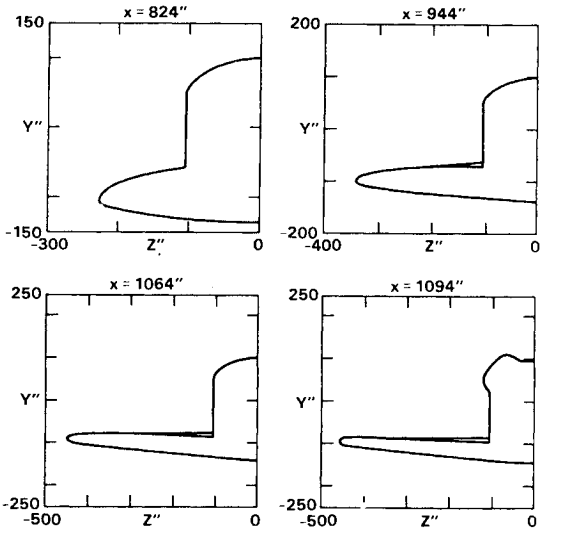

Fig. 17 Modification in wing surface at various $x = \text{const}$ planes; $M_\infty = 1.25$.

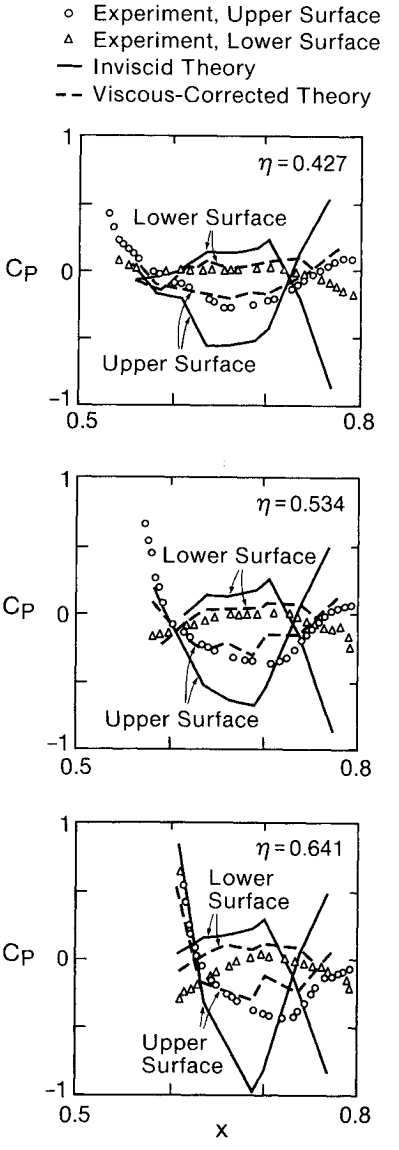

Fig. 18 Inviscid and viscous-corrected chordwise pressures on Orbiter wing; $M_\infty = 1.25$.

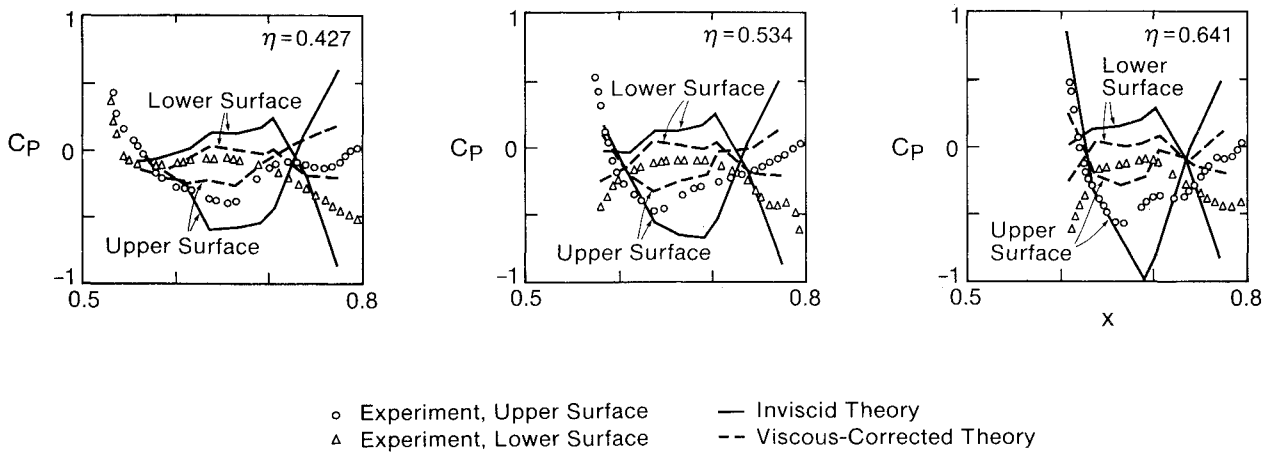

Fig. 19 Inviscid and viscous-corrected chordwise pressures on Orbiter wing: $M_\infty = 0.9$.

body, a simple wing-body combination, and the Shuttle Orbiter. Figure 4 illustrates the comparison of computed result with experiment for a circular cone. The inner and outer solutions are shown along with the added, total pressure distribution. Pressure results for the flow over an elliptic cone for various angles of attack are shown in Fig. 5. Similar results for a parabolic arc of revolution body are illustrated in Figs. 6 and 7. Figures 8 and 9 show off-body pressures for the parabolic arc of revolution body. The predictions are excellent for the flows over these simple bodies.

Figure 10 compares the computed pressure with the experimental values for a simple wing-body combination at the pressure taps shown in the geometry. The off-body pressure and velocities along a line parallel to the axis for two Mach cases are illustrated in Figs. 11 and 12. The computed results for this body are good everywhere except at some "trouble spots" where the geometry variations in the axial direction are very rapid.

Circumferential pressure distributions on the fuselage from the Orbiter calculations are compared with experiments in Fig. 13. The pressure results on the wing are given for various chordwise span stations illustrated in Fig. 14. The predicted pressure results in the rear part of the wing were poor. The discrepancy was attributed to the exclusion of viscous effects. These may be considerable in the aft portion of the wing.

To incorporate viscous effects, a turbulent boundary layer integral method[16] was used, and its displacement effect was used to modify the wing surface. This procedure involves numerical integration of three simultaneous ordinary differential equations. They are the momentum integral equation, the entrainment equation, and the equation for the streamwise rate of change of entrainment coefficient. However, the change in the shape of the wing surface due to the attached boundary layer assumed in the lag-entrainment method[16] was too small to reduce the discrepancies with experiment.

Based on the adverse pressure gradients present, the concept of a separated boundary layer was employed. From qualitative modeling, Figs. 15 and 16 show the modification in the wing surface at various span stations due to a thick separated layer. The original airfoil sections and the modified, thicker ones are given in these figures. A few Orbiter cross-sectional shapes, including the modification, are illustrated in Fig. 17. Figure 18 shows the inviscid and viscous-corrected pressure results for the chordwise upper and lower surface pressure on the wing for $M_\infty = 1.25$. Similar results for $M_\infty = 0.9$ are given in Fig. 19. The improvement in the results due to the qualitative viscous correction is good.

A concurrent study has been conducted to use the slender body theory to predict subsonic flows and is reported in Ref. 17.

Conclusion

Transonic slender body theory was developed to analyze simple and complicated geometries such as the Shuttle Orbiter. For attached flows, the inviscid calculations predicted the pressure distribution with good accuracy. On the rear part of the Orbiter wing where viscous effects such as separation may be important, substantial discrepancies with experiment are evident. To account for this, a viscous correction was applied by modifying the wing surface in a qualitative manner. This improved the comparison between theory and experiment. A next step in this research effort is the incorporation of a more systematic viscous correction model into the inviscid slender body code.

Acknowledgments

This work was sponsored by Rockwell International Space Operations under NASA Contract No. NASA 9-14000. The authors wish to thank T. E. Surber and H. Dresser for their assistance and valuable interactions in this effort.

References

[1]Cole, J. D., "Studies in Transonic Flow I: Transonic Area Rule-Bodies," Univ. of California, Los Angeles, UCLA Rept. UCLA-Eng. 7257, Aug. 1972.

[2]Heaslet, M. A. and Spreiter, J. R., "Three-Dimensional Transonic Flow Theory Applied to Slender Wings and Bodies," NACA Rept. 1318, Sept. 1956.

[3]Malmuth, N. D., Wu, C. C., and Cole, J. D., "Slender Body Theory and Optimization Procedures for Transonic Lifting Bodies," *Journal of Aircraft*, Vol. 21, April 1984, pp. 256-263.

[4]Cheng, H. K. and Hafez, M. M.," Transonic Equivalence Rule; A Nonlinear Problem Involving Lift," *Journal of Fluid Mechanics*, Vol. 72, Pt. 1, 1975, pp. 161-187.

[5]Malmuth, N.D., Wu, C.C., and Cole, J. D., "Slender Body Theory and Space Shuttle Transonic Aerodynamics," AIAA Paper 85-0478, Jan. 1985.

[6]Cole, J. D., *Perturbation Methods in Applied Mathematics*, Blaisdell, Waltham, MA, 1968.

[7]Cole, J. D. and Cook, L. P., *Transonic Aerodynamics*, North Holland, New York, 1986.

[8]Krupp, J. A. and Murman, E. M., "Computation of Transonic Flow Past Lifting Airfoils and Slender Bodies," *AIAA Journal*, Vol. 10, July 1972, pp. 880-886.

[9]Bailey, F. R., "Numerical Calculation of Transonic Flow About Slender Bodies of Revolution," NASA TN D-6582, Dec. 1971.

[10]Ashley, H. and Landahl, M., *Aerodynamics of Wings and Bodies*, Addison-Wesley, Reading, MA, 1965.

[11]Jaswon, M. A. and Symm, G. T., *Integral Equation Methods in Potential Theory and Elastostatics*, Academic, New York, 1977.

[12]Brebbia, C. A., *The Boundary Element Methods for Engineers*, Pentech, London, England, and Halstead Press, New York, 1978.

[13]Brebbia, C. A., Telles, J. C. F., and Wrobel, L. C., *Boundary Element Techniques: Theory and Applications in Engineering*, Springer-Verlag, Berlin, 1984.

[14]Rajagopal, K., Lick, W. J., and Malmuth, N. D., "A Comparative Study of Two Different Boundary Element Methods to Solve Two-Dimensional Potential Problems," *Developments in Mechanics*, Purdue University, Lafayette, IN, Vol. 14a, pp. 373–378.
[15]Kellogg, O. D., *Foundations of Potential Theory*, Springer-Verlag, New York, 1929.
[16]Green, J. E., Weeks, D. J., and Brooman, J. W. F, "Prediction of Turbulent Boundary-Layers and Wakes in Compressible Flow by a Lag-Entrainment Method," Royal Aircraft Establishment, Farnborough, England, Reports and Memorandum No. 3791, Jan. 1973.
[17]Rajagopal, K., Malmuth, N. D., and Lick, W., "A Slender Body Code for Flow Field and Load Prediction – Theory, Application and User's Manual," Rockwell International Science Center, Thousand Oaks, CA, Rept. SCM38514.1, 1987.